Thermocapillary migration of a deformed droplet in the combined vertical temperature gradient and thermal radiation
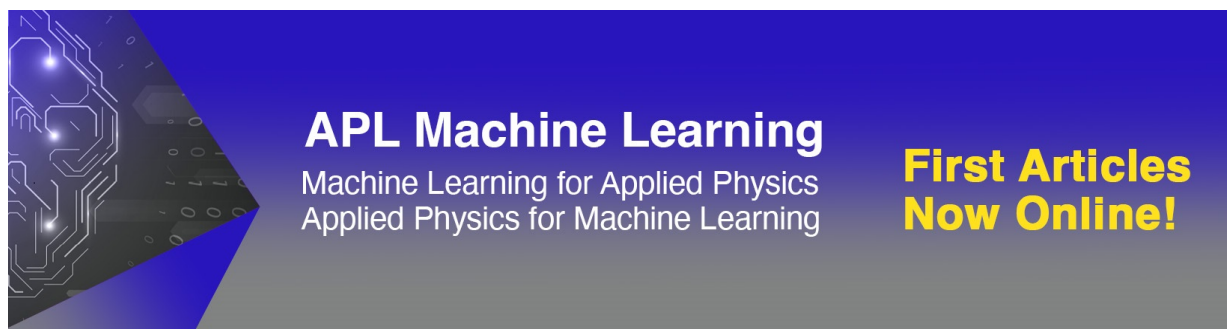
Zuo-Bing Wu (武作兵)

View Online   Export Citation   CrossMark

APL Machine Learning
Machine Learning for Applied Physics
Applied Physics for Machine Learning

First Articles Now Online!

Thermocapillary migration of a deformed droplet in the combined vertical temperature gradient and thermal radiation

View Online   Export Citation   CrossMark

Zuo-Bing Wu (武作兵)[1,2,a] (iD)

AFFILIATIONS

[1]LNM, Institute of Mechanics, Chinese Academy of Sciences, Beijing 100190, China
[2]School of Engineering Science, University of Chinese Academy of Sciences, Beijing 100049, China

[a]Author to whom correspondence should be addressed: wuzb@lnm.imech.ac.cn

ABSTRACT

Thermocapillary migration of a deformed droplet in the combined vertical temperature gradient and thermal radiations with uniform and non-uniform fluxes is first analyzed. The creeping flow solutions show that the deformed droplet has a slender or a cardioid shape, which depends on the form of the radiation flux. The deviation from a sphere depends not only on the viscosity and the conductivity ratios of two-phase fluids but also on capillary and thermal radiation numbers. Moreover, in the roles of interfacial rheology on thermocapillary migration of a deformed droplet, only the surface dilatational viscosity and the surface internal energy can reduce the steady migration velocity, but the surface shear viscosity has not any effects on the steady migration velocity. The surface shear and dilatational viscosities affect the deformation of the droplet by increasing the viscosity ratio of two-phase fluids. The surface internal energy directly reduces the deformation of the droplet. However, the deformed droplet still keeps its original shape without the influence of interfacial rheology. Furthermore, it is found that, based on the net force balance condition of the droplet, the normal stress balance at the interface can be used to determine the steady migration velocity, which is not affected by the surface deformation in the creeping flow. From the expressions of the normal/the tangential stress balance, it can be proved that the surface shear viscosity does not affect the steady migration velocity. The results could not only provide a valuable understanding of thermocapillary migration of a deformed droplet with/without the interfacial rheology in a vertical temperature gradient controlled by thermal radiation but also inspire its potential practical applications in microgravity and microfluidic fields.

Published under an exclusive license by AIP Publishing. https://doi.org/10.1063/5.0142144

I. INTRODUCTION

The migration of a droplet in an external fluid caused by the non-uniform surface tension distribution along the interface between two immiscible fluids under reduced gravity is termed thermocapillary droplet migration. Based on the practical applications of space exploration, studies on the physical mechanism of thermocapillary droplet migration become more and more important. To generate the non-uniform surface tension, two different thermal sources are transmitted through the bulk liquid to the droplet surface. On the one hand, a vertical temperature gradient is added in the bulk liquid by providing the non-uniform temperature distribution along the interface. Young *et al.*[1] studied the thermocapillary migration of a droplet in a vertical temperature gradient field and obtained the droplet migration velocity in zero limits of Reynolds (Re) and Marangoni (Ma) numbers. At small Re and Ma numbers, Bratukhin,[2] Balasubramaniam, and Chai,[3] and Haj-Hariri *et al.*[4] analyzed the deformation of a droplet in the

thermaocapillary migration process and found an ellipsoidal shape with the axis of rotation in the flow direction, the amplitude of which mainly depends on the Weber (We) number and the density ratio of two-phase fluids. With the aid of the vertical temperature gradient in the bulk liquid, the thermocapillary droplet migration at small Re and Ma numbers and its physical mechanisms are understood very well.[5] At moderate and large Ma(Re) numbers, Zhao *et al.*,[6] Alhendal *et al.*,[7] Capobianchi *et al.*,[8] and Kalichetty *et al.*[9,10] numerically simulated thermocapillary migration of a deformed/non-deformed droplet and found that the steady migration velocity decreases as Ma increases in both the ranges of moderate and large Ma numbers. However, Yin *et al.*[11] numerically simulated the thermocapillary migration of a non-deformed droplet and found that as Ma increases, the steady migration velocity decreases/increases in the range of moderate/large Ma numbers. This result is consistent with that obtained numerically by solving the steady governing equations.[12] The qualitative

differences of theoretical, numerical, and experimental results on thermocapillary drop migration at large Ma numbers and their possible reasons are summarized in Ref. 13. On the other hand, the thermal radiation to the droplet surface is another method to provide the non-uniform temperature distribution along the interface. Oliver and DeWitt[14] analyzed the thermocapillary droplet migration under the thermal radiation with a uniform thermal flux at zero limits of Re and Ma numbers and obtained the steady migration velocity. Meanwhile, Rednikov and Ryazantsev[15] independently derived the same results and determined the deformation of the droplet, which depends on the Capillary (Ca) number, the viscosity, and the conductivity ratios of two-phase fluids. At finite Re and Ma numbers, Lopez et al.[16] and Rendondo et al.[17] experimentally investigated thermocapillary droplet migration driven by a laser beam and found the accelerating and steady migration processes of the droplet. Under various forms of illumination with a laser beam, Ryazantsev et al.[18] experimentally controlled the movement of a droplet to push, pull, and hold the stationary droplet. In terms of numerical simulation, Zhang et al.[19] and Gao and Wu[20] found that the steady migration velocity of the droplet decreases as Ma increases. It is clear that, in principle, the laser radiation technology can produce the similar effects by adding the vertical temperature gradient on thermocapillary droplet migration.

In general, the deformation of the moving droplet depends on a lot of factors, such as pressure, viscous stress, interface tension, interfacial rheology, and so on. The above works omit an explicit consideration of the interfacial rheology on interface boundary conditions for a small surface-to-volume ratio. However, when the fluid surface-to-volume ratio increases, the interface is regarded as material in nature. In this case, the interfacial rheology will affect the deformation of the droplet through the force balance on the interface and its terminal velocity.[21] By introducing the interface rheology, Scriven[22] added the effects of the surface dilatational and shear viscosities in the surface stress tensors and derived a general formulation of the dynamics of a Newtonian fluid interface of two-phase fluids. Based on the influence of the stretching and shrinking of surface elements on the temperature of the interfacial layer, Harper et al.[23] and Torres and Herbolzheimer[24] introduced the surface internal energy into the interfacial thermal flux balance and indicated that the effect is significant for the movement of a bubble/drop in low-viscosity liquids at small Re and Peclet (Pe) numbers. By considering the effects of interfacial rheology, Khattari et al.[25] and Balasubramaniam and Subramanian[26] analyzed thermocapillary droplet migration processes at small Re and Ma numbers and found that the surface shear viscosity has not to influence on the steady migration velocities. In recent works, due to the consideration of the complex transport of surfactants along the surface, the movement of a droplet under the influence of interfacial rheology received more attention. Schwalbe et al.,[27] Das and Chakraborty,[28] and Narsimhan[29] show that interfacial rheology can modify the dynamics of a spherical droplet in a plane Poiseuille flow or a Stokes flow and found that the droplet migration velocity is unaffected by the shear viscosity, whereas the dilatational viscosity has a significant effect. Subsequently, Jadhav and Ghosh[30] studied the effect of interfacial kinetics on the settling of a drop in a viscous medium at small Re and Ma numbers and found that stresses originating from interfacial rheology tend to decrease the settling velocity.

Recently, in view of the mechanism of the varied surface tension with temperature, some topics on applications of thermocapillary convection in a confined regime under the laser heating are concerned with the fluid-handling microtechnology.[31,32] Basically, with the decreasing of the length scale in microfluidic devices, the effects of interfacial phenomena become dominant and the local changes of surface tension can be effective to control the growth and movement of droplets. Rybalko et al.,[33] Baroud et al.,[34] Muto et al.,[35] and Xiao et al.[36] proposed the non-contact manipulation techniques of droplets by the light irradiation and applied to move a drop forward and backward/sorting drops in the micro-channels. This is due to a local temperature gradient given by the irradiation of heating light to generate the Marangoni convection around the drop. In terms of the thermocapillary flow at the zero limits of Re and Ma numbers, the forces acting on drops were determined to reveal correspondent physical mechanisms. In the microgravity environment, the action of laser radiation may be taken as the thermal radiation technology to control the thermocapillary droplet migration in the vertical temperature gradient field. It was found that a nonconservative integral thermal flux across the interface exists in the steady migration process, which leads to an unsteady process of thermocapillary droplet migration in the vertical temperature gradient field at large Ma numbers.[37] By adding the thermal radiation on the droplet, the conservative integral thermal flux across the interface in the steady thermocapillary migration at large Ma numbers is reached to show that the steady migration velocity increases with the increasing of Ma number.[38] Based on the manipulation of varied radiation forms, Wu[39] theoretically analyzed and numerically investigated the thermocapillary migration of a non-deformed droplet in a vertical temperature gradient controlled by uniform and non-uniform thermal radiations. The steady migration velocity decreases/increases with the increase of the Ma number/thermal radiation (Tr) number. However, some interesting topics on thermocapillary migration of a deformed droplet in the combined vertical temperature gradient and thermal radiation, such as the effects of uniform and non-uniform thermal radiations on the shape of a droplet, effects of the interfacial rheology on the steady migration velocity, and the shape of droplet, remain to be studied with respect to their physical mechanisms.

In this paper, we first show creeping flow solutions of thermocapillary migration of a deformed droplet in the combined vertical temperature gradient and thermal radiation and determine the dependence of the droplet shape on the physical parameters of two-phase fluids. Then, we investigate the effects of interfacial rheology on the steady migration velocity of the deformed droplet and the shape of the droplet. Section II determines analytical solutions of thermocapillary migration of a deformed droplet in the combined vertical temperature gradient and thermal radiation at zero limits of Re and Ma numbers. Effects of interfacial rheology on thermocapillary migration of a deformed droplet are analyzed in Sec. III. Finally, in Sec. IV, conclusions and discussions are given.

II. CREEPING FLOW SOLUTIONS OF THERMOCAPILLARY MIGRATION OF A DEFORMED DROPLET

Consider a single droplet with a radius $R_0(\mathrm{cm})$ placed in a continuous-phase fluid of unbounded extend under a uniform vertical temperature gradient $G(\mathrm{K/cm})$ and a thermal radiation flux $\Omega(\mathrm{W/cm^2})$, as illustrated in Fig. 1. The direction of the incident radiation is antiparallel to the uniform vertical temperature gradient G.

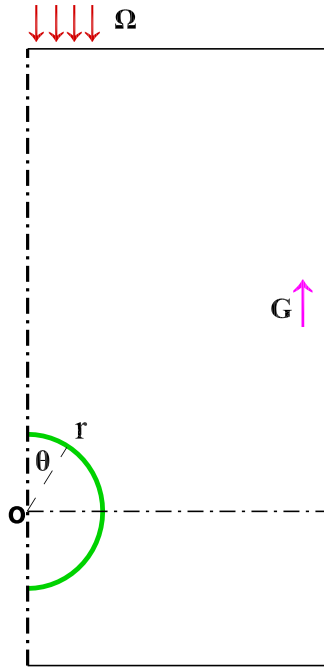**FIG. 1.** A schematic of the thermocapillary droplet migration system under a vertical temperature gradient G and a thermal radiation flux Ω.

The thermal radiation flux $\Omega \, [= \Theta f(\bar{\mathbf{r}}_b)]$ is assumed as a uniform or a wave function with the amplitude $\Theta(\mathrm{W/cm^2})$. The droplet surface and the continuous-phase fluid are assumed as a gray body and transparent to radiation, respectively. Since the gravity is ignored, the droplet moves up due to the non-uniform surface tension $\sigma = \sigma_0 + \sigma_T(T - T_0)$, where $\sigma_0(\mathrm{dyn/cm})$ and $\sigma_T(\mathrm{dyn/cm\,K})$ are the surface tension coefficient at the undisturbed temperature $T_0(\mathrm{K})$ and the changing rate of the interfacial tension between the droplet and the continuous-phase fluid with temperature $T(\mathrm{K})$, respectively. In the modeling assumptions, both fluids are immiscible, and the physical properties are constant. The equations of states for density $\rho_i(\mathrm{g/cm^3})$, viscosity $\mu_i(\mathrm{dyns/cm^2})$, heat conduction $k_i(\mathrm{W/cmK})$, and heat diffusivity $\kappa_i(\mathrm{cm^2/s})$ are written as follows:

$$\frac{d\rho_i}{dt} = \frac{d\mu_i}{dt} = \frac{dk_i}{dt} = \frac{d\kappa_i}{dt} = 0. \tag{1}$$

Symbols with subscripts 1 and 2 denote physical variables and coefficients of the continuous-phase fluid and the droplet, respectively.

By taking the radius of the droplet R_0, the velocity $v_0 = -\sigma_T G R_0/\mu_1$ and $G R_0$ as the reference quantities to make coordinates, velocity and temperature dimensionless, the continuity, momentum and energy equations for the continuous-phase fluid, and the droplet are derived in the Appendix and written in the non-dimensional form as

$$\nabla \cdot \mathbf{v}_i = 0,$$
$$\rho_i \frac{\partial \mathbf{v}_i}{\partial t} + \rho_i \mathbf{v}_i \cdot \nabla \mathbf{v}_i = -\nabla p_i + \frac{\mu_i}{Re} \Delta \mathbf{v}_i, \tag{2}$$
$$\frac{\partial T_i}{\partial t} + \mathbf{v}_i \cdot \nabla T_i = \frac{\kappa_i}{Ma} \Delta T_i,$$

where the symbols $\mathbf{v}_i, p_i, T_i$ represent the velocity, pressure, and temperature of the continuous fluid and the droplet, respectively. The physical coefficients are non-dimensionlized by the quantities of continuous-phase fluid. Re, Ma, Tr, and Ca numbers are, respectively, defined as

$$Re = \frac{\rho_1 v_0 R_0}{\mu_1}, \quad Ma = \frac{v_0 R_0}{\kappa_1}, \quad Tr = \frac{\Theta}{G k_1}, \quad \text{and} \quad Ca = \frac{v_0 \mu}{\sigma_0}. \tag{3}$$

In the following, unless otherwise specified, all physical coefficients, physical quantities, governing equations, and boundary conditions are provided in the non-dimensional form.

At zero limits of Re and Ma numbers, the momentum and energy equations in Eq. (2) are derived in the Appendix and written in an axisymmetric spherical coordinate system (r, θ) moving with the droplet velocity V_∞

$$\mu_i \Delta \mathbf{v}_i = Re \nabla p_i \quad \text{or} \quad E^4 \psi_i = 0,$$
$$\Delta T_i = 0, \tag{4}$$

where

$$E^2 = \frac{\partial^2}{\partial r^2} + \frac{\sin^2 \theta}{r^2} \frac{\partial^2}{\partial(\cos \theta)^2} \tag{5}$$

and ψ_i is the stream functions of the continuous fluid and the droplet. Since a small deformation of the interface in the steady migration process is assumed as $R(\theta) = 1 + Ca\xi(\theta)$ and $Ca \ll 1$, all boundary conditions in the spherical coordinates transformed from the curve coordinates of the interface[2,40] can be truncated at the first order $O(Ca)$. At the place far from the droplet, the velocity and temperature of the continuous-phase fluid should satisfy

$$\mathbf{v}_1(r \to \infty, \theta) \to (-V_\infty \cos \theta, V_\infty \sin \theta),$$
$$T_1(r \to \infty, \theta) \to r \cos \theta. \tag{6}$$

At the droplet surface, the velocities inside and outside the droplet must meet the continuous and impermeable conditions described below

$$v_{r,1}(1, \theta) = v_{r,2}(1, \theta) = 0,$$
$$v_{\theta,1}(1, \theta) = v_{\theta,2}(1, \theta). \tag{7}$$

Meanwhile, the temperatures and the heat fluxes inside and outside the droplet must be continuous and in balance with the thermal radiation as given below, respectively,

$$T_1(1, \theta) = T_2(1, \theta) \tag{8}$$

and

$$\frac{\partial T_1}{\partial r}(1, \theta) + Trf(\theta)\cos\theta = k_2 \frac{\partial T_2}{\partial r}(1, \theta), \quad \theta \in [0, \pi/2],$$
$$\frac{\partial T_1}{\partial r}(1, \theta) = k_2 \frac{\partial T_2}{\partial r}(1, \theta), \quad \theta \in [\pi/2, \pi]. \tag{9}$$

The differences of the tangential and normal stresses between the continuous-phase fluid and the droplet are balanced by the surface tension and its interfacial gradient as written below, respectively,

$$\Pi_{r\theta,1}(1, \theta) - \Pi_{r\theta,2}(1, \theta) = -\frac{1}{Re}\frac{\partial\sigma}{\partial\theta} \tag{10}$$

and

$$\Pi_{rr,1}(1,\theta) - \Pi_{rr,2}(1,\theta) = \frac{2H\sigma}{Re}, \quad (11)$$

where $\sigma = \frac{1}{Ca} - T_1(1,\theta)$, $2H = \frac{2R^2 + 3R'^2 - RR''}{(R^2 + R'^2)^{3/2}} - ctg\theta \frac{R'}{R(R^2 + R'^2)^{1/2}} = 2 - Ca(2\xi + ctg\theta\xi' + \xi'')$, and $\Pi_{r\theta,i} = \frac{\mu_i}{Re}[r\frac{\partial}{\partial r}(\frac{v_{\theta,i}}{r}) + \frac{1}{r}\frac{\partial v_{r,i}}{\partial \theta}]$, $\Pi_{rr,i} = -p_i + \frac{2\mu_i}{Re}\frac{\partial v_{r,i}}{\partial r}$. The deformed droplet in the steady migration process is required to satisfy the following two facts. On the one hand, the volume of the droplet remains unchanged, which demands that

$$\int_0^\pi \xi(\theta)\sin\theta d\theta = 0. \quad (12)$$

On the other hand, the center of mass of the droplet is always fixed at the origin of coordinates, which demands that

$$\int_0^\pi \xi(\theta)\sin\theta\cos\theta d\theta = 0. \quad (13)$$

The shape of the droplet can be, thus, written as

$$R(\theta) = 1 + Ca\xi(\theta) = 1 + Ca\sum_{n=2}^\infty A_n P_n(\cos\theta), \quad (14)$$

where $P_n(\cos\theta)$ is the Legendre polynomial of order n and A_n is an unknown parameter.

In Subsections II A–II C, the thermal radiation fluxes $Trf(\theta)$ with the uniform thermal radiation $f_1 = 1$ and the non-uniform thermal radiations $f_2 = \cos\theta$ and $f_3 = \sin^2\theta$ are taken to analyze creeping flow solutions of thermocapillary migration of a deformed droplet in

the combined vertical temperature gradient and thermal radiation, respectively.

A. Uniform thermal radiation [$f_1(\theta)=1$]

Following the methods for solving the problems for low Re number hydrodynamics,[39,41,42] the solutions of the governing equation (4) satisfying the boundary conditions (6)–(10) with the uniform thermal radiation [$f_1(\theta) = 1$] can be determined as

$$\psi_1 = \frac{V_\infty}{2}(r^2 - r^{-1})\sin^2\theta + \sum_{n=3,odd}^\infty D_n(r^{3-n} - r^{1-n})C_n^{-1/2}(\cos\theta),$$

$$\psi_2 = \frac{3V_\infty}{4}(r^4 - r^2)\sin^2\theta + \sum_{n=3,odd}^\infty D_n(r^{2+n} - r^n)C_n^{-1/2}(\cos\theta), \quad (15)$$

and

$$T_1 = \frac{Tr}{4}r^{-1} + \left[r + \frac{2 - 2k_2 + Tr}{2(2 + k_2)}r^{-2}\right]\cos\theta$$
$$+ \sum_{n=2,even}^\infty a_n r^{-(n+1)}P_n(\cos\theta), \quad (16)$$

$$T_2 = \frac{Tr}{4} + \frac{6 + Tr}{2(2 + k_2)}r\cos\theta + \sum_{n=2,even}^\infty a_n r^n P_n(\cos\theta),$$

where $a_n = \frac{(-1)^{(n-2)/2}(2n+1)Tr}{2[(1+k_2)n+1](n-1)(n+2)}\prod_{j=1}^{n/2}\frac{2j-1}{2j}$ ($n \geq 2$, even), $D_n = \frac{n(n-1)}{2(2n-1)(1+\mu_2)}a_{n-1}$ ($n \geq 3$, odd). $C_n^{-1/2}(s) = \int_s^1 P_{n-1}(x)dx$ is the Gegenbauer polynomial of order n. As an example shown in Fig. 2(a),
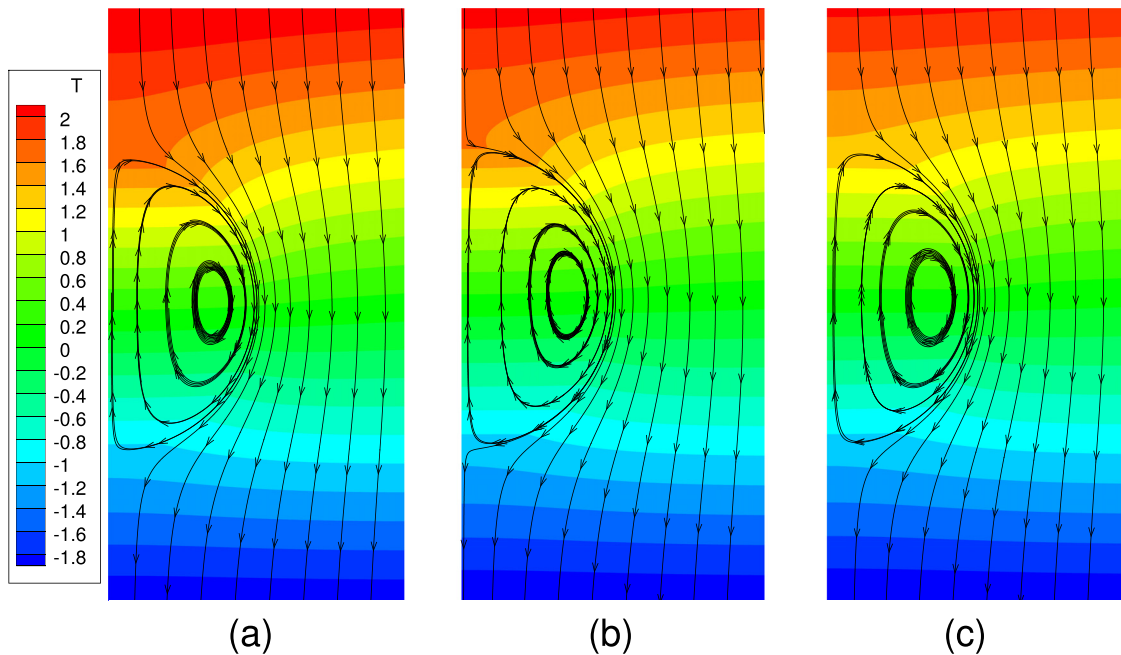

FIG. 2. Streamlines in velocity fields/isotherms in temperature fields described by the Gegenbauer/Legendre polynomial in Eqs. (15), (22), and (29)/Eqs. (16), (23), and (30) truncated at the order $n = 5/4$ for thermocapillary droplet migration in the combined vertical temperature gradient and the thermal radiations (a) $Trf_1(\theta)$, (b) $Trf_2(\theta)$, and (c) $Trf_3(\theta)$ at the zero limits of Re and Ma numbers under $k_2 = \mu_2 = 0.5$ and $Tr = 1$.

when the external streamlines go around the droplet, the Hill's spherical vortex is formed inside the droplet. At the top of the droplet, the heat absorbed by the interface is transported to the continuous-phase fluid and the droplet through heat conduction. The temperature of both fluids near the top of the droplet is, thus, significantly higher than that of other parts. The isotherms at the top of the droplet tend to bend. Moreover, by integrating the radial momentum equations in Eq. (4), both the pressure fields of the continuous-phase fluid and the droplet are as follows:

$$p_1 = -\frac{1}{Re}\sum_{n=3,odd}^{\infty}\frac{2(2n-3)}{n}D_nP_{n-1}(\cos\theta)r^{-n},$$

$$p_2 = \frac{\mu_2}{Re}\left[p_0 - 15V_\infty r\cos\theta\right. \tag{17}$$

$$\left. -\sum_{n=3,odd}^{\infty}\frac{2(2n+1)}{n-1}D_nP_{n-1}(\cos\theta)r^{n-1}\right].$$

The normal stress balance at the interface of Eq. (11) can be rewritten as

$$-p_1 + \frac{2}{Re}\frac{\partial v_{r,1}}{\partial r} + p_2 - \frac{2\mu_2}{Re}\frac{\partial v_{r,2}}{\partial r} = \frac{2H}{Re}\left[\frac{1}{Ca} - T_1(1,\theta)\right]. \tag{18}$$

By substituting the solutions in Eqs. (15)–(17), Eq. (18) is derived as

$$-6V_\infty\cos\theta - \sum_{n=3,odd}^{\infty}\frac{6}{n}D_nP_{n-1}(\cos\theta)$$

$$+\mu_2\left[p_0 - 9V_\infty\cos\theta - \sum_{n=3,odd}^{\infty}\frac{6}{n-1}D_nP_{n-1}(\cos\theta)\right]$$

$$=2\left[\frac{1}{Ca} - \frac{Tr}{4} - \frac{6+Tr}{2(2+k_2)}\cos\theta - \sum_{n=2,even}^{\infty}a_nP_n(\cos\theta)\right.$$

$$\left. +\sum_{n=2}^{\infty}\frac{(n-1)(n+2)}{2}A_nP_n(\cos\theta) + O(Ca)\right], \tag{19}$$

where the first-order term $O(Ca)$ can be truncated. In Eq. (19), the Legendre polynomial coefficients of the same order n on both sides of the equation must be equal. Based on this rule, the following results can be derived from Eq. (19)

$$p_0 = \frac{2}{Ca} - \frac{Tr}{2} \quad (n=0),$$

$$V_{1,\infty} = \frac{6+Tr}{3(2+k_2)(2+3\mu_2)} \quad (n=1),$$

$$A_n = \frac{n+2+(n-1)\mu_2}{(n-1)(n+2)(2n+1)(1+\mu_2)}a_n \quad (n\geq 2, even),$$

$$A_n = 0 \quad (n\geq 2, odd),$$

where $a_n \to O(n^{-2})$ and $A_n \to O(n^{-4})$ if $n(\geq 2, even)\to\infty$. It reveals that A_n monotonously decreases as $n(\geq 2, even)$ increases. The shape of the deformed droplet can be, thus, written as
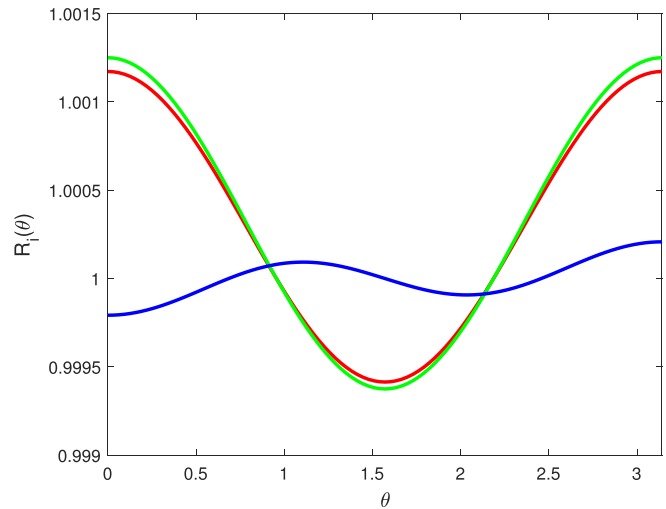

FIG. 3. The shape $R_i(\theta)$ of the deformed droplet vs $\theta \in [0,\pi]$ for thermocapillary migration in the combined vertical temperature gradient and the thermal radiation $Trf_i(\theta)$ at the zero limits of Re and Ma numbers under $k_2 = \mu_2 = 0.5$, $Ca = 0.1$, and $Tr = 1$. The uniform radiation function $f_1 = 1$ and the non-uniform radiation functions $f_2 = \cos\theta$ and $f_3 = \sin^2\theta$ are denoted by the red, green, and blue lines, respectively.

$$R_1(\theta) = 1 + Ca\xi(\theta) = 1 + Ca\sum_{n=2,even}^{\infty}A_nP_n(\cos\theta)$$

$$\approx 1 + \frac{(4+\mu_2)CaTr}{64(3+2k_2)(1+\mu_2)}P_2(\cos\theta). \tag{21}$$

It is noted that the deformed droplet attains a slender sphere $[\xi(0) = \xi(\pi) > 0$ and $\xi(\pi/2) < 0]$, as shown in Fig. 3. The slender sphere in the (r,θ) coordinate plane has a mirror symmetry about the line $\theta = \pi/2$. Meanwhile, under the uniform thermal radiation $Trf_1 = 1$, the steady migration velocity $V_{\infty,1}$ is increased by 16.6% as an example given in Table I.

B. Non-uniform thermal radiation $[f_2(\theta)=\cos\theta]$

Using the above methods, the solutions of the governing equation (4) satisfying the boundary conditions (6)–(10) with the non-uniform thermal radiation $[f_2(\theta) = \cos\theta]$ can be determined as

TABLE I. The steady migration velocity $V_{i,\infty}$ of the droplet in the vertical temperature gradient without/with the thermal radiation $Trf_i(\theta)$ ($f_1 = 1$, $f_2 = \cos\theta$, and $f_3 = \sin^2\theta$) at the zero limits of Re and Ma numbers under $k_2 = \mu_2 = 0.5$ and $Tr = 0/1$. The effects of interfacial rheology with $\kappa_s = E_s = 0.2$ on $V_{i,\infty}$ are also included for the comparison. The number in parentheses/square brackets after entry is the incremental percentage based on the droplet migration velocity without/with the thermal radiation ($Tr = 0/1$ and $\kappa_s = E_s = 0$).

	$V_{1,\infty}$	$V_{2,\infty}$	$V_{3,\infty}$
$Tr = 0$, $\kappa_s = E_s = 0$	0.229	0.229	0.229
$Tr = 1$, $\kappa_s = E_s = 0$	0.267 (16.6)	0.257 (12.2)	0.244 (6.6)
$Tr = 1$, $\kappa_s = E_s = 0.2$	0.230 [−13.9]	0.222 [−13.6]	0.210 [−13.9]

$$\psi_1 = \frac{V_\infty}{2}(r^2 - r^{-1})\sin^2\theta + D_3(1 - r^{-2})C_3^{-1/2}(\cos\theta)$$
$$+ \sum_{n=4,even}^{\infty} D_n(r^{3-n} - r^{1-n})C_n^{-1/2}(\cos\theta),$$

$$\psi_2 = \frac{3V_\infty}{4}(r^4 - r^2)\sin^2\theta + D_3(r^5 - r^3)C_3^{-1/2}(\cos\theta)$$
$$+ \sum_{n=4,even}^{\infty} D_n(r^{2+n} - r^n)C_n^{-1/2}(\cos\theta), \tag{22}$$

and

$$T_1 = \frac{Tr}{6}r^{-1} + \left[r + \frac{8 - 8k_2 + 3Tr}{8(2 + k_2)}r^{-2}\right]\cos\theta$$
$$+ \frac{Tr}{3(3 + 2k_2)}r^{-3}P_2(\cos\theta)$$
$$+ \sum_{n=3,odd}^{\infty} a_n r^{-(n+1)}P_n(\cos\theta), \tag{23}$$

$$T_2 = \frac{Tr}{6} + \frac{3(8 + Tr)}{8(2 + k_2)}r\cos\theta + \frac{Tr}{3(3 + 2k_2)}r^2 P_2(\cos\theta)$$
$$+ \sum_{n=3,odd}^{\infty} a_n r^n P_n(\cos\theta),$$

where $a_n = \frac{(-1)^{(n+1)/2}(2n+1)Tr}{[(1+k_2)n+1](n-2)(n+1)(n+3)}\prod_{j=1}^{(n-1)/2}\frac{2j-1}{2j}$ $(n \geq 3, \text{odd})$, $D_3 = \frac{Tr}{5(3+2k_2)(1+\mu_2)}$, and $D_n = \frac{n(n-1)}{2(2n-1)(1+\mu_2)}a_{n-1}$ $(n \geq 4, \text{even})$. As an example shown in Fig. 2(b), the velocity fields are similar to those for the uniform thermal radiation f_1. However, the temperature of both fluids near the top of the droplet is lower than that for the uniform thermal radiation f_1 due to the non-uniform radiation f_2. Moreover, by integrating the radial momentum equations in Eq. (4), both the pressure fields of the continuous-phase fluid and the droplet are as follows:

$$p_1 = -\frac{1}{Re}\left[2D_3 P_2(\cos\theta)r^{-3}\right.$$
$$\left. + \sum_{n=4,even}^{\infty}\frac{2(2n-3)}{n}D_n P_{n-1}(\cos\theta)r^{-n}\right], \tag{24}$$

$$p_2 = \frac{\mu_2}{Re}\left[p_0 - 15V_\infty r\cos\theta - 5D_3 P_2(\cos\theta)r^2\right.$$
$$\left. - \sum_{n=4,even}^{\infty}\frac{2(2n+1)}{n-1}D_n P_{n-1}(\cos\theta)r^{n-1}\right].$$

The normal stress balance at the interface of Eq. (11) can be rewritten as

$$-p_1 + \frac{2}{Re}\frac{\partial v_{r,1}}{\partial r} + p_2 - \frac{2\mu_2}{Re}\frac{\partial v_{r,2}}{\partial r} = \frac{2H}{Re}\left[\frac{1}{Ca} - T_1(1,\theta)\right]. \tag{25}$$

By substituting the solutions in Eqs. (22)–(24), Eq. (25) is derived as

$$-6V_\infty\cos\theta - 2D_3 P_2(\cos\theta) - \sum_{n=4,even}^{\infty}\frac{6}{n}D_n P_{n-1}(\cos\theta)$$
$$+ \mu_2\left[p_0 - 9V_\infty\cos\theta - 3D_3 P_2(\cos\theta)\right.$$
$$\left. - \sum_{n=4,even}^{\infty}\frac{6}{n-1}D_n P_{n-1}(\cos\theta)\right]$$
$$= 2\left[\frac{1}{Ca} - \frac{Tr}{6} - \frac{3(8 + Tr)}{8(2 + k_2)}\cos\theta - \frac{Tr}{3(3 + 2k_2)}P_2(\cos\theta)\right.$$
$$- \sum_{n=3,odd}^{\infty} a_n P_n(\cos\theta) + \sum_{n=2}^{\infty}\frac{(n-1)(n+2)}{2}A_n P_n(\cos\theta)$$
$$\left. + O(Ca)\right], \tag{26}$$

where the first-order term $O(Ca)$ can be truncated. In Eq. (26), the Legendre polynomial coefficients of the same order n on both sides of the equation must be equal. Based on this rule, the following results can be derived from Eq. (26):

$$p_0 = \frac{2}{Ca} - \frac{Tr}{3} \quad (n = 0),$$
$$V_{2,\infty} = \frac{8 + Tr}{4(2 + k_2)(2 + 3\mu_2)} \quad (n = 1),$$
$$A_2 = \frac{(4 + \mu_2)Tr}{60(3 + 2k_2)(1 + \mu_2)} \quad (n = 2), \tag{27}$$
$$A_n = \frac{n + 2 + (n-1)\mu_2}{(n-1)(n+2)(2n+1)(1 + \mu_2)}a_n \quad (n \geq 3, \text{odd}),$$
$$A_n = 0 \quad (n \geq 3, \text{even}),$$

where $a_n \to O(n^{-3})$ and $A_n \to O(n^{-5})$, if $n(\geq 3, \text{odd}) \to \infty$. It reveals that A_n monotonously decreases as $n(\geq 3, \text{odd})$ increases. The shape of the deformed droplet can be, thus, written as

$$R_2(\theta) = 1 + Ca\xi(\theta)$$
$$= 1 + CaA_2 P_2(\cos\theta) + Ca\sum_{n=3,odd}^{\infty} A_n P_n(\cos\theta)$$
$$\approx 1 + \frac{(4 + \mu_2)CaTr}{60(3 + 2k_2)(1 + \mu_2)}P_2(\cos\theta). \tag{28}$$

It is noted that the deformed droplet attains a slender sphere $[\xi(0) = \xi(\pi) > 0$ and $\xi(\pi/2) < 0]$ as shown in Fig. 3. The slender sphere in the (r, θ) coordinate plane has a mirror symmetry about the line $\theta = \pi/2$. Meanwhile, under the non-uniform thermal radiation $Trf_2 = \cos\theta$, the steady migration velocity $V_{\infty,2}$ is increased by 12.2% as an example given in Table I.

In comparison between the uniform thermal radiation $f_1 = 1$ and the non-uniform thermal radiation $f_2 = \cos(\theta)$, they have a similar heat flux distribution absorbed by the upper interface of the droplet. As shown in Fig. 4, the higher/lower heat flux is concentrated on the arc of $\theta \in [0, \pi/4]/\theta \in [\pi/4, \pi/2]$. It produces the similar deformation of the droplet for thermocapillary migration in the combined vertical temperature gradient and thermal radiation.
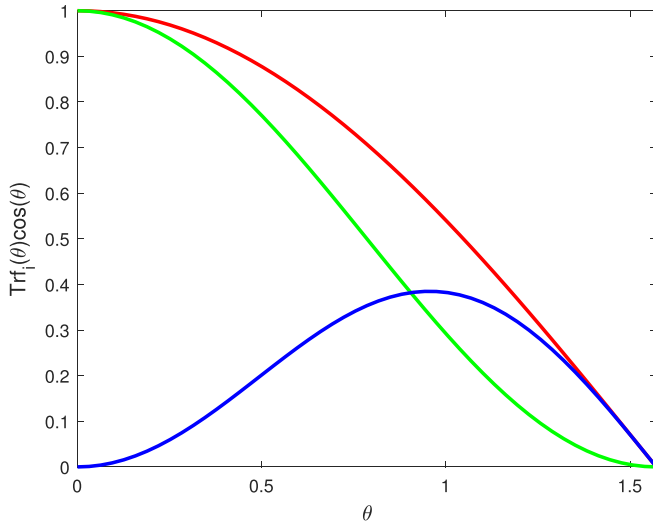
FIG. 4. Heat fluxes $Tr f_i(\theta) \cos\theta$ absorbed by the upper interface of the droplet vs $\theta \in [0, \pi/2]$ at $Tr = 1$ for the uniform thermal radiation $f_1 = 1$ and the non-uniform thermal radiations $f_2 = \cos\theta$ and $f_3 = \sin^2\theta$ are denoted by the red, green, and blue lines, respectively.

C. Non-uniform thermal radiation [$f_3(\theta) = \sin^2\theta$]

Following the above derivations, the solutions of the governing equation (4) satisfying the boundary conditions (6)–(10) with the non-uniform thermal radiation [$f_3(\theta) = \sin^2\theta$] can be determined as

$$\psi_1 = \frac{V_\infty}{2}(r^2 - r^{-1})\sin^2\theta + D_4(r^{-1} - r^{-3})C_4^{-1/2}(\cos\theta)$$
$$+ \sum_{n=5,odd}^{\infty} D_n(r^{3-n} - r^{1-n})C_n^{-1/2}(\cos\theta),$$

$$\psi_2 = \frac{3V_\infty}{4}(r^4 - r^2)\sin^2\theta + D_4(r^6 - r^4)C_4^{-1/2}(\cos\theta)$$
$$+ \sum_{n=5,odd}^{\infty} D_n(r^{2+n} - r^n)C_n^{-1/2}(\cos\theta),$$

$$(29)$$

and

$$T_1 = \frac{Tr}{8}r^{-1} + \left[r + \frac{5 - 5k_2 + Tr}{5(2 + k_2)}r^{-2}\right]\cos\theta$$
$$- \frac{Tr}{5(4 + 3k_2)}r^{-4}P_3(\cos\theta)$$
$$+ \sum_{n=4,even}^{\infty} a_n r^{-(n+1)}P_n(\cos\theta),$$

$$T_2 = \frac{Tr}{8} + \frac{15 + Tr}{5(2 + k_2)}r\cos\theta - \frac{Tr}{5(4 + 3k_2)}r^3 P_3(\cos\theta)$$
$$+ \sum_{n=4,even}^{\infty} a_n r^n P_n(\cos\theta),$$

$$(30)$$

where $a_n = \frac{(-1)^{n/2}(n-2)(n+3)(2n+1)Tr}{2[(1+k_2)n+1](n-3)(n-1)(n+2)(n+4)}\prod_{j=1}^{n/2}\frac{2j-1}{2j}$ $(n \geq 4, even)$, $D_4 = -\frac{6Tr}{35(4+3k_2)(1+\mu_2)}$, and $D_n = \frac{n(n-1)}{2(2n-1)(1+\mu_2)}a_{n-1}$ $(n \geq 5, odd)$. As an example shown in Fig. 2(c), the velocity fields are similar to those for the uniform/non-uniform thermal radiation f_1/f_2. However, the temperature

of both fluids near the top of the droplet is further reduced. Compared with the uniform/non-uniform thermal radiation f_1/f_2, the isotherms at the top of the droplet tend to be straight. Moreover, by integrating the radial momentum equations in Eq. (4), both the pressure fields of the continuous-phase fluid and the droplet are as follows:

$$p_1 = -\frac{1}{Re}\left[\frac{5}{2}D_4 P_3(\cos\theta)r^{-4}\right.$$
$$\left. + \sum_{n=5,odd}^{\infty}\frac{2(2n-3)}{n}D_n P_{n-1}(\cos\theta)r^{-n}\right],$$

$$p_2 = \frac{\mu_2}{Re}\left[p_0 - 15V_\infty r\cos\theta - 6D_4 P_3(\cos\theta)r^3\right.$$
$$\left. - \sum_{n=5,odd}^{\infty}\frac{2(2n+1)}{n-1}D_n P_{n-1}(\cos\theta)r^{n-1}\right].$$

$$(31)$$

The normal stress balance at the interface of Eq. (11) can be rewritten as

$$-p_1 + \frac{2}{Re}\frac{\partial v_{r,1}}{\partial r} + p_2 - \frac{2\mu_2}{Re}\frac{\partial v_{r,2}}{\partial r} = \frac{2H}{Re}\left[\frac{1}{Ca} - T_1(1, \theta)\right]. \quad (32)$$

By substituting the solutions in Eqs. (29)–(31), Eq. (32) is derived as

$$- 6V_\infty \cos\theta - \frac{3}{2}D_4 P_3(\cos\theta) - \sum_{n=5,odd}^{\infty}\frac{6}{n}D_n P_{n-1}(\cos\theta)$$

$$+ \mu_2\left[p_0 - 9V_\infty \cos\theta - 2D_4 P_3(\cos\theta)\right.$$

$$\left. - \sum_{n=5,odd}^{\infty}\frac{6}{n-1}D_n P_{n-1}(\cos\theta)\right]$$

$$= 2\left[\frac{1}{Ca} - \frac{Tr}{8} - \frac{15 + Tr}{5(2 + k_2)}\cos\theta + \frac{Tr}{5(4 + 3k_2)}P_3(\cos\theta)\right.$$

$$- \sum_{n=4,even}^{\infty}a_n P_n(\cos\theta) + \sum_{n=2}^{\infty}\frac{(n-1)(n+2)}{2}$$

$$\left. \times A_n P_n(\cos\theta) + O(Ca)\right],$$

$$(33)$$

where the first-order term $O(Ca)$ can be truncated. In Eq. (33), the Legendre polynomial coefficients of the same order n on both sides of the equation must be equal. Based on this rule, the following results can be derived from Eq. (33),

$$p_0 = \frac{2}{Ca} - \frac{Tr}{4} \quad (n = 0),$$

$$V_{3,\infty} = \frac{2(15 + Tr)}{15(2 + k_2)(2 + 3\mu_2)} \quad (n = 1),$$

$$A_2 = 0 \quad (n = 2),$$

$$A_3 = -\frac{(5 + 2\mu_2)Tr}{350(4 + 3k_2)(1 + \mu_2)} \quad (n = 3),$$

$$A_n = \frac{n + 2 + (n-1)\mu_2}{(n-1)(n+2)(2n+1)(1 + \mu_2)}a_n \quad (n \geq 4, even),$$

$$A_n = 0 \quad (n \geq 4, odd),$$

$$(34)$$

where $a_n \to O(n^{-2})$ and $A_n \to O(n^{-4})$, if $n(\geq 4, \text{even}) \to \infty$. It reveals that A_n monotonously decreases as $n(\geq 4, \text{even})$ increases. The shape of the deformed droplet can be, thus, written as

$$R_3(\theta) = 1 + Ca\xi(\theta)$$

$$= 1 + CaA_3 P_3(\cos\theta) + Ca \sum_{n=4,even}^{\infty} A_n P_n(\cos\theta)$$

$$\approx 1 - \frac{(5+2\mu_2)CaTr}{350(4+3k_2)(1+\mu_2)} P_3(\cos\theta). \quad (35)$$

It is noted that the deformed droplet attains a cardioid sphere $[\xi(0) = -\xi(\pi) < 0$ and $\xi(\pi/2) = 0]$ as shown in Fig. 3. The cardioid sphere in the (r,θ) coordinate plane has a central symmetry about the point $(r,\theta) = (1, \pi/2)$. Meanwhile, under the non-uniform thermal radiation $Trf_3 = \sin^2\theta$, the steady migration velocity $V_{\infty,3}$ is increased by 6.6% as an example given in Table I.

To compare with the uniform thermal radiation $f_1 = 1$ and the non-uniform thermal radiation $f_2 = \cos(\theta)$, the non-uniform thermal radiation $f_3 = \sin^2(\theta)$ has a different heat flux distribution absorbed by the upper interface of the droplet. As shown in Fig. 4, the higher/lower heat flux is concentrated on the arc of $\theta \in [\pi/4, \pi/2]/\theta \in [0, \pi/4]$. It causes the different deformation of the droplet for thermocapillary migration in the combined vertical temperature gradient and thermal radiation. In comparison among the uniform thermal radiation f_1 and the non-uniform thermal radiations f_2 and f_3, the deformation of the droplet depends not only on the viscosity ratio μ_2 and the conductivity ratio k_2 of the two-phase fluids but also on Ca and Tr numbers. Meanwhile, the thermal radiation flux Trf_i can significantly increase the steady migration velocity $V_{i,\infty}$ of the droplet as an example given in Table I. Moreover, based on the net force balance condition of the droplet ($F_z = 4\pi D_2 = 0$), the normal stress balance at the interface in Eq. (11), i.e., the matched Legendre polynomial coefficients of $P_1(\cos\theta)$ on both sides of Eqs. (19), (26), and (33), can be used to determine the steady migration velocity $V_{i,\infty}$. In other words, considering the droplet deformation does not affect the steady migration velocity $V_{i,\infty}$. This result is agreement with those obtained in the investigating thermocapillary migration of a deformed droplet in a vertical temperature gradient/under the thermal radiation at the zero limits of Re[2–4] and Ma numbers.[15]

III. EFFECTS OF INTERFACIAL RHEOLOGY ON THERMOCAPILLARY MIGRATION OF A DEFORMED DROPLET

From the analysis by Happer et al.[23] and Scriven,[22] the interfacial rheology can affect both the heat flux and the stress balances at the interface. The heat fluxes inside and outside the droplet must be continuous and in balance with the thermal radiation and the interfacial rheology (accommodating the stretching and shrinkage of the interface related to the surface internal energy e_s per unit area and the surface tension σ) as follows:

$$\frac{\partial T_1}{\partial r}(1,\theta) + Trf(\theta)\cos\theta = k_2 \frac{\partial T_2}{\partial r}(1,\theta) + \frac{E_s}{\sin\theta}\frac{\partial}{\partial\theta}$$
$$\times [v_\theta(1,\theta)\sin\theta], \quad \theta \in [0, \pi/2],$$
$$\frac{\partial T_1}{\partial r}(1,\theta) = k_2 \frac{\partial T_2}{\partial r}(1,\theta) + \frac{E_s}{\sin\theta}\frac{\partial}{\partial\theta}$$
$$\times [v_\theta(1,\theta)\sin\theta], \quad \theta \in [\pi/2, \pi], \quad (36)$$

where $E_s(= e_s - \sigma)$, which is non-dimensionalized by $-\mu_1 k_1/\sigma_T$, is assumed as a positive constant over the droplet surface. The differences of the tangential and normal stresses at the interface are balanced by the surface tension, its interfacial gradient, and the interfacial rheology (considering effects of the surface viscosity) as written below, respectively,

$$\Pi_{r\theta,1}(1,\theta) - \Pi_{r\theta,2}(1,\theta)$$
$$= -\frac{1}{Re}\frac{\partial\sigma}{\partial\theta} - \frac{2\mu_s}{Re}v_\theta(1,\theta) - \frac{\kappa_s + \mu_s}{Re}\frac{\partial}{\partial\theta}$$
$$\times \left\{\frac{1}{\sin\theta}\frac{\partial}{\partial\theta}[v_\theta(1,\theta)\sin\theta]\right\} \quad (37)$$

and

$$\Pi_{rr,1}(1,\theta) - \Pi_{rr,2}(1,\theta) = \frac{2H\sigma}{Re} + \frac{2\kappa_s}{Re}\frac{1}{\sin\theta}\frac{\partial}{\partial\theta}[v_\theta(1,\theta)\sin\theta], \quad (38)$$

where μ_s and κ_s, which are non-dimensionalized by $\mu_1 R_0$, denote the surface shear and dilatational viscosities, respectively.

In Subsections III A–III C, the thermal radiation fluxes $Trf(\theta)$ with the uniform thermal radiation $f_1 = 1$ and the non-uniform thermal radiations $f_2 = \cos\theta$ and $f_3 = \sin^2\theta$ are taken to investigate the effects of interfacial rheology on thermocapillary migration of a deformed droplet in the combined vertical temperature gradient and thermal radiation, respectively.

A. Uniform thermal radiation [$f_1(\theta)=1$]

Following the methods for solving the problems for low Re number hydrodynamics,[39,41,42] the solutions of the governing equation (4) satisfying the boundary conditions (6)–(8), (36), and (37) with the uniform thermal radiation [$f_1(\theta) = 1$] can be determined as

$$\psi_1 = \frac{V_\infty}{2}(r^2 - r^{-1})\sin^2\theta + \sum_{n=3,odd}^{\infty} D_n(r^{3-n} - r^{1-n})C_n^{-1/2}(\cos\theta),$$

$$\psi_2 = \frac{3V_\infty}{4}(r^4 - r^2)\sin^2\theta + \sum_{n=3,odd}^{\infty} D_n(r^{2+n} - r^n)C_n^{-1/2}(\cos\theta),$$

$$(39)$$

and

$$T_1 = \frac{Tr}{4}r^{-1} + \left[r + \frac{2 - 2k_2 + Tr - 6E_sV_\infty}{2(2+k_2)}r^{-2}\right]\cos\theta$$
$$+ \sum_{n=2,even}^{\infty} a_n r^{-(n+1)} P_n(\cos\theta), \quad (40)$$

$$T_2 = \frac{Tr}{4} + \frac{6 + Tr - 6E_sV_\infty}{2(2+k_2)}r\cos\theta + \sum_{n=2,even}^{\infty} a_n r^n P_n(\cos\theta),$$

where $D_n = \frac{(-1)^{(n-1)/2}n(n-1)(2n-1)Tr}{4\{[k_2(n-1)+n]\lambda_n + n(n-1)E_s\}(n-2)(n+1)}\prod_{j=1}^{(n-1)/2}\frac{2j-1}{2j}$ $(n \geq 3, \text{odd})$, $\lambda_n = (2n-1)(1+\mu_2) + n(n-1)\kappa_s + (n-2)(n+1)\mu_s$, and $a_n = \frac{2\lambda_{n+1}}{n(n+1)}$ $\times D_{n+1}(n \geq 2, \text{even})$. As an example shown in Fig. 5(a), the steady velocity and temperature fields are similar to those in Fig. 2(a), which reveals that the influence of the interfacial rheology on them is not obvious. Through the net force balance condition [$F_z = 2\pi \times \int_0^\pi [\Pi_{rr,1}(1,\theta)\cos\theta - \Pi_{r\theta,1}(1,\theta)\sin\theta]\sin\theta d\theta = 0$] and the shear
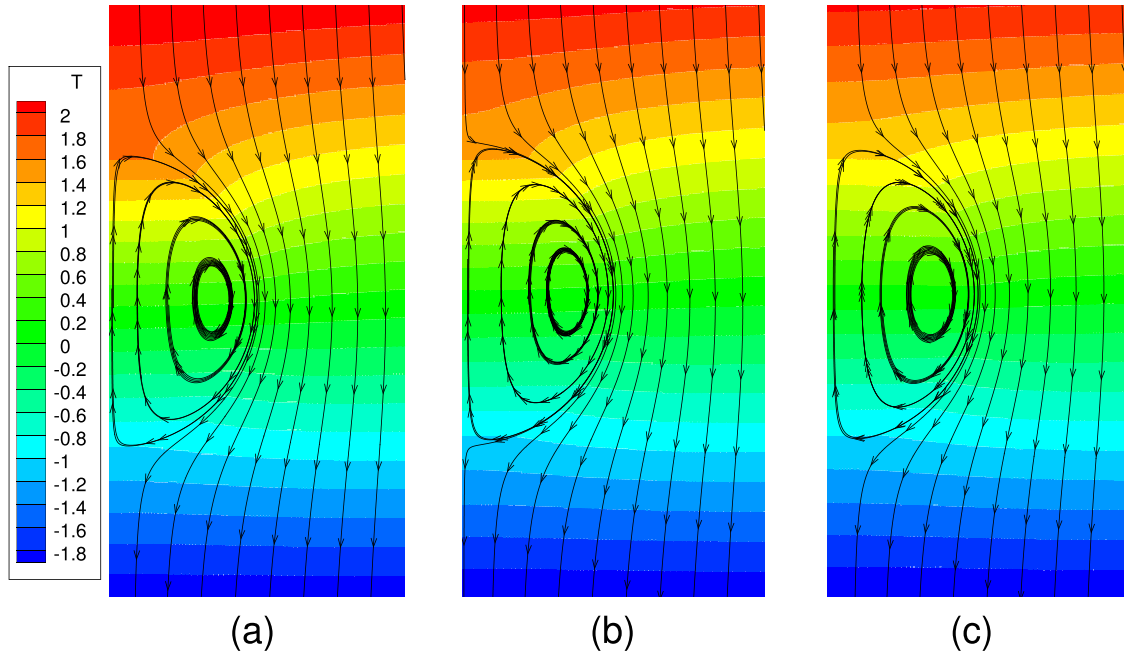
FIG. 5. Streamlines in velocity fields/isotherms in temperature fields described by the Gegenbauer/Legendre polynomial in Eqs. (39), (46), and (53)/Eqs. (40), (47), and (54) truncated at the order $n = 5/4$ for thermocapillary migration of a droplet associated with interfacial rheology in the combined vertical temperature gradient and the thermal radiations (a) $Trf_1(\theta)$, (b) $Trf_2(\theta)$, and (c) $Trf_3(\theta)$ at the zero limits of Re and Ma numbers under $k_2 = \mu_2 = 0.5$, $k_s = \mu_s = E_s = 0.2$, and $Tr = 1$.

stress balance condition at the interface in Eq. (37), the steady migration velocity is then obtained and written as

$$V_{1,\infty}^{ir} = \frac{6 + Tr}{3[(2 + k_2)(2 + 3\mu_2 + 2\kappa_s) + 2E_s]}. \quad (41)$$

The normal stress balance at the interface of Eq. (38) can be rewritten as

$$-p_1 + \frac{2}{Re}\frac{\partial v_{r,1}}{\partial r} + p_2 - \frac{2\mu_2}{Re}\frac{\partial v_{r,2}}{\partial r}$$
$$= \frac{2H}{Re}\left[\frac{1}{Ca} - T_1(1,\theta)\right] + \frac{2\kappa_s}{Re}\frac{1}{\sin\theta}\frac{\partial}{\partial\theta}[v_\theta(1,\theta)\sin\theta]. \quad (42)$$

By substituting the solutions in Eqs. (39) and (40) and the corresponding pressure fields p_i [having the same expressions in Eq. (17)], Eq. (42) is derived as

$$-6V_\infty\cos\theta - \sum_{n=3,odd}^{\infty}\frac{6}{n}D_nP_{n-1}(\cos\theta)$$
$$+ \mu_2\left[p_0 - 9V_\infty\cos\theta - \sum_{n=3,odd}^{\infty}\frac{6}{n-1}D_nP_{n-1}(\cos\theta)\right]$$
$$= 2\left[\frac{1}{Ca} - \frac{Tr}{4} - \frac{6 + Tr - 6E_sV_\infty}{2(2 + k_2)}\cos\theta - \sum_{n=2,even}^{\infty}a_nP_n(\cos\theta)\right.$$
$$\left.+ \sum_{n=2}^{\infty}\frac{(n-1)(n+2)}{2}A_nP_n(\cos\theta) + O(Ca)\right]$$
$$+ 2\kappa_s\left[3V_\infty\cos\theta + 2\sum_{n=3,odd}^{\infty}D_nP_{n-1}(\cos\theta)\right], \quad (43)$$

where the first-order term $O(Ca)$ can be truncated. In Eq. (43), the Legendre polynomial coefficients of the same order n on both sides of the equation must be equal. Based on this rule, the following results can be derived from Eq. (43),

$$p_0 = \frac{2}{Ca} - \frac{Tr}{2} \quad (n = 0),$$

$$V_{1,\infty}^{ir} = \frac{6 + Tr}{3[(2 + k_2)(2 + 3\mu_2 + 2\kappa_s) + 2E_s]} \quad (n = 1),$$

$$A_n = \frac{(n-1)\mu_2 + (n+2)[1 + 2(n-1)\mu_s]}{\lambda_{n+1}(n-1)(n+2)}a_n \quad (n \ge 2, even),$$

$$A_n = 0 \quad (n \ge 2, odd), \quad (44)$$

where $a_n \to O(n^{-2})$ and $A_n \to O(n^{-4})$ if $n(\ge 2, even) \to \infty$. It reveals that A_n monotonously decreases as $n(\ge 2, even)$ increases. Thus, the shape of the deformed droplet is written as

$$R_1^{ir}(\theta) = 1 + Ca\xi(\theta)$$
$$= 1 + CaA_2P_2(\cos\theta) + Ca\sum_{n=4,even}^{\infty}A_nP_n(\cos\theta)$$
$$\approx 1 + \frac{5(4 + \mu_2 + 8\mu_s)CaTr}{64\{(3 + 2k_2)[5(1 + \mu_2) + 6\kappa_s + 4\mu_s] + 6E_s\}}P_2(\cos\theta). \quad (45)$$

It is noted that the steady migration velocity $V_{1,\infty}^{ir}$ and the shape $R_1^{ir}(\theta)$ of the deformed droplet return $V_{1,\infty}$ and $R_1(\theta)$ in Eqs. (20) and (21), respectively, when the surface shear viscosity μ_s, the surface dilatational viscosity κ_s and the surface internal energy E_s are zero. Only
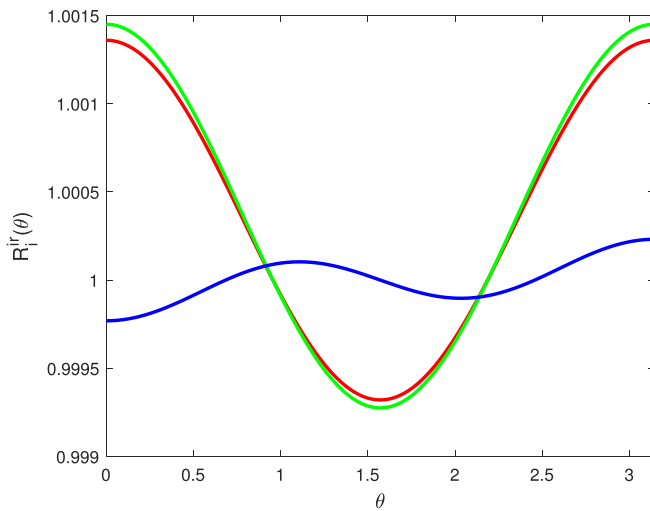
FIG. 6. The shape $R_i^{ir}(\theta)$ of the deformed droplet vs $\theta \in [0, \pi]$ for thermocapillary migration in the combined vertical temperature gradient and the thermal radiation $Trf_i(\theta)$ at the zero limits of Re and Ma numbers under $k_2 = \mu_2 = 0.5$, $\kappa_s = \mu_s = E_s = 0.2$, $Ca = 0.1$, and $Tr = 1$. The uniform radiation function $f_1 = 1$ and the non-uniform radiation functions $f_2 = \cos \theta$ and $f_3 = \sin^2 \theta$ are denoted by the red, green, and blue lines, respectively.

the surface dilatational viscosity κ_s and the surface internal energy E_s can reduce the steady migration speed $V_{1,\infty}^{ir}$, but the surface shear viscosity μ_s does not affect the steady migration velocity $V_{1,\infty}^{ir}$. As an example given in Table I, under the effects of interfacial rheology, $V_{\infty,1}^{ir}$ is decreased by 13.9%. Moreover, the surface shear viscosity μ_s and the surface dilatational viscosity κ_s affect the deviation value $\xi(\theta)$ from a sphere by increasing the viscosity ratio μ_2 of two-phase fluids. The surface internal energy E_s directly reduces the deviation value $\xi(\theta)$ from a sphere. However, the deformed droplet still attains a slender sphere as shown in Fig. 6.

B. Non-uniform thermal radiation [$f_2(\theta) = \cos \theta$]

Using the above methods, the solutions of the governing equation (4) satisfying the boundary conditions(6)–(8), (36), and (37) with the non-uniform thermal radiation [$f_2(\theta) = \cos \theta$] can be determined as

$$
\begin{aligned}
\psi_1 &= \frac{V_\infty}{2}(r^2 - r^{-1})\sin^2\theta + D_3(1 - r^{-2})C_3^{-1/2}(\cos\theta) \\
&\quad + \sum_{n=4,even}^{\infty} D_n(r^{3-n} - r^{1-n})C_n^{-1/2}(\cos\theta), \\
\psi_2 &= \frac{3V_\infty}{4}(r^4 - r^2)\sin^2\theta + D_3(r^5 - r^3)C_3^{-1/2}(\cos\theta) \\
&\quad + \sum_{n=4,even}^{\infty} D_n(r^{2+n} - r^n)C_n^{-1/2}(\cos\theta),
\end{aligned}
\tag{46}
$$

and

$$
\begin{aligned}
T_1 &= \frac{Tr}{6}r^{-1} + \left[r + \frac{8 - 8k_2 + 3Tr - 24E_sV_\infty}{8(2+k_2)}r^{-2}\right]\cos\theta \\
&\quad + \frac{Tr - 6E_sD_3}{3(3+2k_2)}r^{-3}P_2(\cos\theta) \\
&\quad + \sum_{n=3,odd}^{\infty} a_n r^{-(n+1)}P_n(\cos\theta),
\end{aligned}
\tag{47}
$$

$$
\begin{aligned}
T_2 &= \frac{Tr}{6} + \frac{3(8 + Tr - 8E_sV_\infty)}{8(2+k_2)}r\cos\theta \\
&\quad + \frac{Tr - 6E_sD_3}{3(3+2k_2)}r^2 P_2(\cos\theta) + \sum_{n=3,odd}^{\infty} a_n r^n P_n(\cos\theta),
\end{aligned}
$$

where $D_3 = \frac{Tr}{(3+2k_2)\lambda_3 + 6E_s}$, $D_n = \frac{(-1)^{n/2}n(n-1)(2n-1)Tr}{2\{[k_2(n-1)+n]\lambda_n+n(n-1)E_s\}(n-3)n(n+2)}$ $\times \Pi_{j=1}^{(n-2)/2}\frac{2j-1}{2j}$ ($n \geq 4$, even), $\lambda_n = (2n-1)(1+\mu_2) + n(n-1)\kappa_s$ $+(n-2)(n+1)\mu_s$, and $a_n = \frac{2\lambda_{n+1}}{n(n+1)}D_{n+1}$ ($n \geq 3$, odd). As an example shown in Fig. 5(b), the steady velocity and temperature fields are similar to those in Fig. 2(b), which reveals that the influence of the interfacial rheology on them is not obvious. Through the net force balance condition $\{F_z = 2\pi\int_0^\pi[\Pi_{rr,1}(1,\theta)\cos\theta - \Pi_{r\theta,1}(1,\theta)\sin\theta]\sin\theta d\theta = 0\}$ and the shear stress balance condition at the interface in Eq. (37), the steady migration velocity is then obtained and written as

$$
V_{2,\infty}^{ir} = \frac{8 + Tr}{4[(2+k_2)(2 + 3\mu_2 + 2\kappa_s) + 2E_s]}.
\tag{48}
$$

The normal stress balance at the interface of Eq. (38) can be rewritten as

$$
\begin{aligned}
&-p_1 + \frac{2}{Re}\frac{\partial v_{r,1}}{\partial r} + p_2 - \frac{2\mu_2}{Re}\frac{\partial v_{r,2}}{\partial r} \\
&= \frac{2H}{Re}\left[\frac{1}{Ca} - T_1(1,\theta)\right] + \frac{2\kappa_s}{Re}\frac{1}{\sin\theta}\frac{\partial}{\partial\theta}[v_\theta(1,\theta)\sin\theta].
\end{aligned}
\tag{49}
$$

By substituting the solutions in Eqs. (46) and (47) and the corresponding pressure fields p_i [having the same expressions in Eq. (24)], Eq. (49) is derived as

$$
\begin{aligned}
&-6V_\infty\cos\theta - 2D_3P_2(\cos\theta) - \sum_{n=4,even}^{\infty}\frac{6}{n}D_nP_{n-1}(\cos\theta) \\
&\quad + \mu_2\left[p_0 - 9V_\infty\cos\theta - 3D_3P_2(\cos\theta)\right. \\
&\qquad\left. - \sum_{n=4,even}^{\infty}\frac{6}{n-1}D_nP_{n-1}(\cos\theta)\right] \\
&= 2\left[\frac{1}{Ca} - \frac{Tr}{6} - \frac{3(8 + Tr - 8E_sV_\infty)}{8(2+k_2)}\cos\theta - \frac{Tr - 6E_sD_3}{3(2+2k_2)}P_2(\cos\theta)\right. \\
&\qquad\left. - \sum_{n=3,odd}^{\infty}a_nP_n(\cos\theta) + \sum_{n=2}^{\infty}\frac{(n-1)(n+2)}{2}A_nP_n(\cos\theta) + O(Ca)\right] \\
&\quad + 2\kappa_s\left[3V_\infty\cos\theta + 2D_3P_2(\cos\theta) + 2\sum_{n=4,even}^{\infty}D_nP_{n-1}(\cos\theta)\right],
\end{aligned}
\tag{50}
$$

where the first-order term $O(Ca)$ can be truncated. In Eq. (50), the Legendre polynomial coefficients of the same order n on both sides of the equation must be equal. Based on this rule, the following results can be derived from Eq. (50)

$$p_0 = \frac{2}{Ca} - \frac{Tr}{3} \quad (n = 0),$$

$$V_{2,\infty}^{ir} = \frac{8 + Tr}{4[(2+k_2)(2+3\mu_2+2\kappa_s)+2E_s]} \quad (n = 1),$$

$$A_2 = \frac{4 + \mu_2 + 8\mu_s}{12} D_3 \quad (n = 2), \tag{51}$$

$$A_n = \frac{(n-1)\mu_2 + (n+2)[1 + 2(n-2)\mu_s]}{\lambda_{n+1}(n-1)(n+2)} a_n \quad (n \geq 3, \text{odd}),$$

$$A_n = 0 \quad (n \geq 3, \text{even}),$$

where $a_n \to O(n^{-3})$ and $A_n \to O(n^{-5})$ if $n(\geq 3, \text{odd}) \to \infty$. It reveals that A_n monotonously decreases as $n(\geq 3, \text{odd})$ increases. Thus, the shape of the deformed droplet is written as

$$R_2^{ir}(\theta) = 1 + Ca\xi(\theta)$$

$$= 1 + CaA_2P_2(\cos\theta) + Ca\sum_{n=3,odd}^{\infty} A_nP_n(\cos\theta)$$

$$\approx 1 + \frac{(4 + \mu_2 + 8\mu_s)CaTr}{12\{(3+2k_2)[5(1+\mu_s)+6\kappa_s+4\mu_s]+6E_s\}}P_2(\cos\theta). \tag{52}$$

It is noted that the steady migration velocity $V_{2,\infty}^{ir}$ and the shape $R_2^{ir}(\theta)$ of the deformed droplet return $V_{2,\infty}$ and $R_2(\theta)$ in Eqs. (27) and (28), respectively, when the surface shear viscosity μ_s, the surface dilational viscosity κ_s, and the surface internal energy E_s are zero. Under the effects of interfacial rheology, the steady migration velocity $V_{2,\infty}^{ir}$ is reduced. As an example given in Table I, $V_{\infty,2}^{ir}$ is decreased by 13.6%. The effects of the interfacial rheology parameters on the steady migration velocity $V_{2,\infty}^{ir}$ and the shape $R_2^{ir}(\theta)$ of the deformed droplet for the non-uniform thermal radiation f_2 are similar to those for the uniform thermal radiation f_1. Meanwhile, although the deviation value $\xi(\theta)$ from a sphere is changed, the deformed droplet still attains a slender sphere as shown in Fig. 6.

C. Non-uniform thermal radiation [$f_3(\theta) = \sin^2\theta$]

Following the above derivations, the solutions of the governing equation (4) satisfying the boundary conditions (6)–(8), (36), and (37) with the non-uniform thermal radiation [$f_3(\theta) = \sin^2\theta$] can be determined as

$$\psi_1 = \frac{V_\infty}{2}(r^2 - r^{-1})\sin^2\theta + D_4(r^{-1} - r^{-3})C_4^{-1/2}(\cos\theta)$$

$$+ \sum_{n=5,odd}^{\infty} D_n(r^{3-n} - r^{1-n})C_n^{-1/2}(\cos\theta),$$

$$\psi_2 = \frac{3V_\infty}{4}(r^4 - r^2)\sin^2\theta + D_4(r^6 - r^4)C_4^{-1/2}(\cos\theta)$$

$$+ \sum_{n=5,odd}^{\infty} D_n(r^{2+n} - r^n)C_n^{-1/2}(\cos\theta), \tag{53}$$

and

$$T_1 = \frac{Tr}{8}r^{-1} + \left[r + \frac{5 - 5k_2 + Tr - 15E_sV_\infty}{5(2+k_2)}r^{-2}\right]\cos\theta$$

$$- \frac{Tr + 10E_sD_4}{5(4+3k_2)}r^{-4}P_3(\cos\theta) + \sum_{n=4,even}^{\infty} a_nr^{-(n+1)}P_n(\cos\theta), \tag{54}$$

$$T_2 = \frac{Tr}{8} + \frac{15 + Tr - 15E_sV_\infty}{5(2+k_2)}r\cos\theta$$

$$- \frac{Tr + 10E_sD_4}{5(4+3k_2)}r^3P_3(\cos\theta) + \sum_{n=4,even}^{\infty} a_nr^nP_n(\cos\theta),$$

where $D_4 = -\frac{6Tr}{5[(4+3k_2)\lambda_4+12E_s]},$ $D_n = \frac{(-1)^{(n-1)/2}(n-3)(n-1)n(n+2)(2n-1)Tr}{4\{[k_2(n-1)+n]\lambda_n+n(n-1)E_s\}(n-4)(n-2)(n+1)(n+3)}\prod_{j=1}^{(n-1)/2}\frac{2j-1}{2j}$ $(n \geq 5, \text{odd})$, $\lambda_n = (2n-1)(1+\mu_2) + n(n-1)\kappa_s + (n-2)(n+1)\mu_s$, and $a_n = \frac{2\lambda_{n+1}}{n(n+1)}D_{n+1}(n \geq 4, \text{even})$. As an example shown in Fig. 5(c), the steady velocity and temperature fields are similar to those in Fig. 2(c), which reveals that the influence of the interfacial rheology on them is not obvious. Through the net force balance condition $\{F_z = 2\pi\int_0^\pi[\Pi_{rr,1}(1,\theta)\cos\theta - \Pi_{r\theta,1}(1,\theta)\sin\theta]\sin\theta d\theta = 0\}$ and the shear stress balance condition at the interface in Eq. (37), the steady migration velocity is then obtained and written as

$$V_\infty = \frac{2(15 + Tr)}{15[(2+k_2)(2+3\mu_2+2\kappa_s)+2E_s]}. \tag{55}$$

The normal stress balance at the interface of Eq. (38) can be rewritten as

$$- p_1 + \frac{2}{Re}\frac{\partial v_{r,1}}{\partial r} + p_2 - \frac{2\mu_2}{Re}\frac{\partial v_{r,2}}{\partial r}$$

$$= \frac{2H}{Re}\left[\frac{1}{Ca} - T_1(1,\theta)\right] + \frac{2\kappa_s}{Re}\frac{1}{\sin\theta}\frac{\partial}{\partial\theta}[v_\theta(1,\theta)\sin\theta]. \tag{56}$$

By substituting the solutions in Eqs. (53) and (54) and the corresponding pressure fields p_i [having the same expressions in Eq. (31)], Eq. (56) is derived as

$$- 6V_\infty\cos\theta - \frac{3}{2}D_4P_3(\cos\theta) - \sum_{n=5,odd}^{\infty}\frac{6}{n}D_nP_{n-1}(\cos\theta)$$

$$+ \mu_2\left[p_0 - 9V_\infty\cos\theta - 2D_4P_3(\cos\theta)\right.$$

$$\left. - \sum_{n=5,odd}^{\infty}\frac{6}{n-1}D_nP_{n-1}(\cos\theta)\right]$$

$$= 2\left[\frac{1}{Ca} - \frac{Tr}{8} - \frac{15 + Tr - 15E_sV_\infty}{5(2+k_2)}\cos\theta + \frac{Tr + 10E_sD_4}{5(4+3k_2)}P_3(\cos\theta)\right.$$

$$\left. - \sum_{n=4,even}^{\infty}a_nP_n(\cos\theta) + \sum_{n=2}^{\infty}\frac{(n-1)(n+2)}{2}A_nP_n(\cos\theta) + O(Ca)\right]$$

$$+ 2\kappa_s\left[3V_\infty\cos\theta + 2D_4P_3(\cos\theta) + 2\sum_{n=5,odd}^{\infty}D_nP_{n-1}(\cos\theta)\right], \tag{57}$$

where the first-order term $O(Ca)$ can be truncated. In Eq. (57), the Legendre polynomial coefficients of the same order n on both sides of the equation must be equal. Based on this rule, the following results can be derived from Eq. (57)

$$p_0 = \frac{2}{Ca} - \frac{Tr}{4} \quad (n = 0),$$

$$V_{3,\infty}^{ir} = \frac{2(15 + Tr)}{15[(2 + k_2)(2 + 3\mu_2 + 2\kappa_s) + 2E_s]} \quad (n = 1),$$

$$A_2 = 0 \quad (n = 2),$$

$$A_3 = \frac{5 + 2\mu_2 + 20\mu_s}{60} D_4 \quad (n = 3),$$

$$A_n = \frac{(n-1)\mu_2 + (n+2)[1 + 2(n-2)\mu_s]}{\lambda_{n+1}(n-1)(n+2)} a_n \quad (n \geq 4, \text{even}),$$

$$A_n = 0 \quad (n \geq 4, \text{odd}),$$

(58)

where $a_n \rightarrow O(n^{-2})$ and $A_n \rightarrow O(n^{-4})$ if $n(\geq 4, \text{even}) \rightarrow \infty$. It reveals that A_n monotonously decreases as $n(\geq 4, \text{even})$ increases. Thus, the shape of the deformed droplet is written as

$$R_3^{ir}(\theta) = 1 + Ca\xi(\theta)$$

$$= 1 + CaA_3 P_3(\cos\theta) + Ca \sum_{n=4, even}^{\infty} A_n P_n(\cos\theta)$$

$$\approx 1 - \frac{(5 + 2\mu_2 + 20\mu_s)CaTr}{50\{(4 + 3k_2)[7(1 + \mu_2) + 12\kappa_s + 10\mu_s] + 12E_s\}}$$

$$\times P_3(\cos\theta).$$

(59)

It is noted that the steady migration velocity $V_{3,\infty}^{ir}$ and the shape $R_3^{ir}(\theta)$ of the deformed droplet return $V_{3,\infty}$ and $R_3(\theta)$ in Eqs. (34) and (35), respectively, when the surface shear viscosity μ_s, the surface dilatational viscosity κ_s, and the surface internal energy E_s are zero. In terms of the effects of the interfacial rheology, the steady migration velocity $V_{3,\infty}^{ir}$ is decreased by 13.9% as an example given in Table I. The effects of the interfacial rheology parameters on the steady migration velocity $V_{3,\infty}^{ir}$ and the shape $R_3^{ir}(\theta)$ of the deformed droplet for the non-uniform thermal radiation f_3 are similar to those for the uniform thermal radiation f_1 or the non-uniform thermal radiation f_2. Meanwhile, although the deviation value $\xi(\theta)$ from a sphere is changed, the deformed droplet still attains a cardioid sphere as shown in Fig. 6.

It is further confirmed that even under the influence of interfacial rheology, based on the net force balance condition of the droplet ($F_z = 4\pi D_2 = 0$), the normal stress balance at the interface in Eq. (38), i.e., the matched Legendre polynomial coefficients of $P_1(\cos\theta)$ on both sides of Eqs. (43), (50), and (57), can be still used to determine the steady migration velocity $V_{i,\infty}^{ir}$. In other words, considering the droplet deformation does not affect the steady migration velocity $V_{i,\infty}^{ir}$. This result is in agreement with those obtained in the investigating thermocapillary migration of a deformed droplet with the interfacial rheology in a vertical temperature gradient at the zero limits of Re and Ma numbers.[26,40] Meanwhile, from the above fact, it is easy to understand the effects of the interfacial rheology in the steady migration velocity $V_{i,\infty}^{ir}$. On the one hand, since the surface shear viscosity μ_s is not involved in the normal stress balance at the interface in Eq. (38), it cannot affect the steady migration velocity $V_{i,\infty}^{ir}$. On the other hand, due to the interfacial rheology, the tangential stress balance at the interface in Eq. (37) is derived as

$$\Pi_{r\theta,1}(1,\theta) - \Pi_{r\theta,2}(1,\theta) + \frac{1}{Re}\frac{\partial\sigma}{\partial\theta}$$

$$= -\frac{2\mu_s}{Re} v_\theta(1,\theta) - \frac{\kappa_s + \mu_s}{Re}\frac{\partial}{\partial\theta}\left\{\frac{1}{\sin\theta}\frac{\partial}{\partial\theta}[v_\theta(1,\theta)\sin\theta]\right\}$$

$$= \frac{3\kappa_s}{Re} V_\infty \sin\theta + \frac{2}{Re}\sum_{n=3}^{\infty}[n(n-1)\kappa_s + (n+1)(n-2)\mu_s]$$

$$\times D_n C_n^{-1/2}(\cos\theta)/\sin\theta,$$

(60)

where the surface shear viscosity μ_s disappears in the coefficient of the second-order Gegenbauer polynomial $C_2^{-1/2}(\cos\theta)/\sin\theta = \sin\theta/2$ on the right-hand side. The surface shear viscosity μ_s does not affect the steady migration velocity $V_{i,\infty}^{ir}$, which is determined by matching the second-order Gegenbauer polynomial coefficients of both sides in Eq. (60).

In the interfacial rheology parameters, only the surface dilatational viscosity κ_s and the surface internal energy E_s have significant roles on the steady migration speed $V_{i,\infty}^{ir}$. These results are in agreement with those obtained in the investigating influence of the interfacial rheology on the thermocapillary droplet migration process,[26] the surfactant-laden droplet dynamics without/with the temperature field in Poiseuille flow[27,28] and in the Stokes flow.[29] As an example in Fig. 5 and Table I, the effects of interfacial rheology are not obvious to change the topological properties of the velocity and temperature fields but can significantly decrease the steady migration velocity of the droplet.

IV. CONCLUSIONS AND DISCUSSIONS

In this paper, first, the thermocapillary migration of a deformed droplet in a vertical temperature gradient and thermal radiations with uniform and non-uniform fluxes at zero limits of Re and Ma numbers is analyzed. In the creeping flow solutions, the deformed droplet has a slender or a cardioid shape, which depends on the form of the thermal radiation. For the uniform thermal radiation $f_1 = 1$ and the non-uniform radiation $f_2 = \cos\theta$, the shape of the deformed droplet is a slender. For the non-uniform radiation $f_3 = \sin^2\theta$, the shape of the deformed droplet is a cardioid. The deviation from a sphere depends not only on the viscosity and the conductivity ratios of two-phase fluids but also on Ca and Tr numbers.

Moreover, the roles of interfacial rheology on thermocapillary migration of a deformed droplet are shown. Only the surface dilatational viscosity and the surface internal energy can reduce the steady migration velocity, but the surface shear viscosity has not any effect on the steady migration velocity. The surface shear and the dilatational viscosities affect the deformation of the droplet by increasing the viscosity ratio of two-phase fluids. The surface internal energy directly reduces the deformation of the droplet. However, the deformed droplet still keeps its original shape without the influence of interfacial rheology.

Furthermore, it is found that, based on the net force balance condition of the droplet, the normal stress balance at the interface can be used to determine the steady migration velocity, which is not affected by the surface deformation in the creeping flow. From the expressions of the normal/the tangential stress balance, it can be proved that the surface shear viscosity does not affect the steady migration velocity.

Up to now, the droplet migration experiments under adding the vertical temperature field or the action of laser radiation have been summarized in the introduction, where any experiments in the combined two actions are not found. However, to eliminate the qualitative differences among the theoretical, numerical, and experimental results of thermocapillary droplet migration with the vertical temperature gradient at large Ma numbers and understand their physical mechanisms, some proposals from the theoretical and numerical works (such as controlling thermocapillary droplet migration in a vertical temperature gradient by the thermal radiation to quickly reach the steady-state migration in the limited test zones[43,44]) can be useful explorations to provide possible implementation approaches and predict results for the experiments of thermocapillary droplet migration in the combined two actions. Meanwhile, in the absence of the experimental validation, some analytical results under the combined two actions in the paper are qualitatively consistent with the previous results under two separate actions, which can be used as an auxiliary proof to validate the results.

Overall, these findings not only improve the understanding of thermocapillary migration of a deformed droplet with/without the interfacial rheology in the combined vertical temperature gradient and thermal radiation but also pave the way for optimizing the form of the thermal radiation to control thermocapillary migration of a deformed droplet, which is of great significance for potential practical applications in the microgravity and microfluidic fields.

AUTHOR DECLARATIONS
Conflict of Interest

The authors have no conflicts to disclose.

Author Contributions

Zuo-Bing Wu: Formal analysis (lead); Funding acquisition (lead); Writing – original draft (lead); Writing – review & editing (lead).

DATA AVAILABILITY

The data that support the findings of this study are available from the corresponding author upon reasonable request.

APPENDIX: NON-DIMENSIONALIZATION OF THE CONTINUITY, MOMENTUM, AND ENERGY EQUATIONS FOR THE CONTINUOUS-PHASE FLUID AND THE DROPLET

The continuity, momentum, and energy equations for the continuous-phase fluid and the droplet in a laboratory coordinate system $\mathbf{r}$(cm) are written as

$$\frac{\partial \rho_i}{\partial t} + \nabla \cdot (\rho_i \mathbf{v}_i) = 0,$$

$$\frac{\partial \rho_i \mathbf{v}_i}{\partial t} + \nabla \cdot (\rho_i \mathbf{v}_i \mathbf{v}_i) = -\nabla p_i + \nabla \cdot [\mu_i (\nabla \mathbf{v}_i + \nabla \mathbf{v}_i^T)], \quad (A1)$$

$$\frac{\partial T_i}{\partial t} + \nabla \cdot (\mathbf{v}_i T_i) = \frac{\kappa_i}{k_i} \nabla \cdot (k_i \nabla T_i),$$

where the symbols $\mathbf{v}_i(\text{cm/s})$, $p_i(\text{dyn/cm}^2)$, $T_i(\text{K})$ represent the velocity, pressure, and temperature, respectively. By taking the radius of the droplet R_0, the velocity $v_0 = -\sigma_T G R_0 / \mu_1$, and $G R_0$ as the reference quantities, the coordinates $\mathbf{r}$, velocity $\mathbf{v}_i$, and temperature T_i are non-dimensionalized as

$$\mathbf{r}^* = \mathbf{r}/R_0, \quad \mathbf{v}_i^* = \mathbf{v}_i/v_0, \quad T_i^* = T_i/(G R_0). \quad (A2)$$

Meanwhile, the physical coefficients (density ρ_i, dynamic viscosity μ_i, thermal conductivity k_i, and thermal diffusivity κ_i) are non-dimensionlized by the quantities of continuous-phase fluid and written as

$$\rho_i^* = \rho_i/\rho_1, \quad \mu_i^* = \mu_i/\mu_1, \quad k_i^* = k_i/k_1, \quad \kappa_i^* = \kappa_i/\kappa_1. \quad (A3)$$

Under the assumption of constant physical coefficients in Eq. (1), Eq. (A1) is rewritten in the non-dimensional form as

$$\nabla^* \cdot \mathbf{v}_i^* = 0,$$

$$\rho_i^* \frac{\partial \mathbf{v}_i^*}{\partial t^*} + \rho_i^* \mathbf{v}_i^* \cdot \nabla^* \mathbf{v}_i^* = -\nabla^* p_i^* + \frac{\mu_i^*}{Re} \Delta^* \mathbf{v}_i^*, \quad (A4)$$

$$\frac{\partial T_i^*}{\partial t^*} + \mathbf{v}_i^* \cdot \nabla^* T_i^* = \frac{\kappa_i^*}{Ma} \Delta^* T_i^*,$$

where $t^* = t/(R_0/v_0)$, $\nabla^* = R_0 \nabla$, $p_i^* = p_i/(\rho_1 v_0^2)$, $\nabla^* \cdot (\rho_i^* \mathbf{v}_i^* \mathbf{v}_i^*) = \rho_i^* [(\nabla^* \cdot \mathbf{v}_i^*) \mathbf{v}_i^*] + (\mathbf{v}_i^* \cdot \nabla^*) \mathbf{v}_i^*] = \rho_i^* \mathbf{v}_i^* \cdot \nabla^* \mathbf{v}_i^*$, $\nabla^* \cdot [\mu_i^* (\nabla^* \mathbf{v}_i^* + \nabla^* \mathbf{v}_i^{*T})] = \mu_i^* \nabla^{*2} \mathbf{v}_i^* = \mu_i^* \Delta^* \mathbf{v}_i^*$.

At zero limits of Re and Ma numbers, the momentum and energy equations in Eq. (A4) are simplified in the coordinate system moving with the droplet as

$$Re \nabla p_i = \mu_i \Delta \mathbf{v}_i,$$
$$\Delta T_i = 0. \quad (A5)$$

Since then, the asterisks "$*$" for the non-dimensional quantities are omitted for convenience. Under the axisymmetric assumption, stream function $\psi_i(r, \theta)$ in a spherical coordinate system (r, θ, ϕ) with a constant ϕ is introduced to generate the velocity field

$$\mathbf{v}_i = (v_{r,i}, v_{\theta,i}, v_{\phi,i}) = \left(-\frac{1}{r^2 \sin\theta} \frac{\partial \psi}{\partial \theta}, \frac{1}{r \sin\theta} \frac{\partial \psi_i}{\partial r}, 0 \right), \quad (A6)$$

which satisfies the continuous equation in Eq. (A4). The curl of the velocity field $\mathbf{v}_i$ is derived as

$$\nabla \times \mathbf{v}_i = \left(0, 0, \frac{1}{r \sin\theta} E^2 \psi_i \right), \quad (A7)$$

where the operator E^2 is defined as

$$E^2 = \frac{\partial^2}{\partial r^2} + \frac{1}{r^2} \frac{\partial^2}{\partial \theta^2} - \frac{\cot\theta}{r^2} \frac{\partial}{\partial \theta} = \frac{\partial^2}{\partial r^2} + \frac{\sin^2\theta}{r^2} \frac{\partial^2}{\partial (\cos\theta)^2}. \quad (A8)$$

By using the continuous equation in Eq. (A4), the momentum equation in Eq. (A5) can be rewritten as

$$Re\nabla p_i = \mu_i \Delta \mathbf{v}_i = -\mu_i \nabla \times (\nabla \times \mathbf{v}_i), \tag{A9}$$

where $\Delta \mathbf{v}_i = \nabla^2 \mathbf{v}_i = \nabla(\nabla \cdot \mathbf{v}_i) - \nabla \times (\nabla \times \mathbf{v}_i)$. By taking the curl on both sides of Eq. (A9) to eliminate the pressure term and substituting Eq. (A7), the following equation can be finally obtained,

$$E^4 \psi_i = 0. \tag{A10}$$

REFERENCES

[1]N. O. Young, J. S. Goldstein, and M. J. Block, "The motion of bubbles in a vertical temperature gradient," J. Fluid Mech. **6**, 350 (1959).

[2]Y. K. Bratukhin, "Thermocapillary drift of a droplet of viscous liquid," Fluid Dyn. **10**, 833 (1975).

[3]R. Balasubramaniam and A.-T. Chai, "Thermocapillary migration of droplets: An exact solution for small Marangoni numbers," J. Coll. Interface Sci. **119**, 531 (1987).

[4]H. Haj-Hariri, A. Nadim, and A. Borhan, "Effects of inertia on the thermocapillary velocity of a drop," J. Coll. Interface Sci. **140**, 277 (1990).

[5]R. S. Subramanian, R. Balasubramaniam, and G. Wozniak, "Fluid mechanics of bubbles and drops," in *Physics of Fluids in Microgravity*, edited by R. Monti (Taylor & Francis, 2001).

[6]J. F. Zhao, L. Zhang, Z. D. Li, and W. T. Qin, "Topological structure evolvement of flow and temperature fields in deformable drop Marangoni migration in microgravity," Int. J. Heat Mass Transfer **54**, 4655 (2011).

[7]Y. Albendal, A. Turan, and A. Kalendar, "Thermocapillary migration of an isolated droplet and interaction of two droplet in zero gravity," Acta Astronaut. **126**, 265 (2016).

[8]P. Capobianchi, M. Lappa, and M. S. Oliveira, "Walls and domain shape effects on the thermal Marangoni migration of three-dimensional droplets," Phys. Fluids **29**, 112102 (2017).

[9]S. S. Kalichetty, T. Sundarajan, and A. Pattamatta, "Thermocapillary migration and interaction dynamics of droplets in a constricted domain," Phys. Fluids **31**, 022106 (2019).

[10]S. S. Kalichetty, T. Sundararajan, and A. Pattamatta, "Effect of wall proximity on the lateral thermocapillary migration of droplet rising in a quiescent liquid," Phys. Fluids **33**, 022107 (2021).

[11]Z. Yin, L. Chang, W. Hu, Q. Li, and H. Wang, "Numerical simulations on thermocapillary migration of nondeformable droplets with large Marangoni numbers," Phys. Fluids **24**, 092101 (2012).

[12]X. Ma, R. Balasubramiam, and R. S. Subramanian, "Numerical simulation of thermocapillary drop motion with internal circulation," Numer. Heat Transfer, Part A **35**, 291 (1999).

[13]Z. Yin, Z.-B. Wu, and W. R. Hu, "Thermocapillary migration of drops and bubbles," *Advances in Microgravity Science*, edited by W. R. Hu (Transworld Research Network, 2009).

[14]D. L. R. Oliver and K. J. Dewitt, "Surface tension driven flows for a droplet in a microgravity environment," Int. J. Heat Mass Transfer **31**, 1534 (1988).

[15]A. Y. Rednikov and Y. S. Ryzzantsev, "Thermocapillary motion of a droplet under the action of radiation," J. Appl. Mech. Tech. Phys. **30**, 337 (1989).

[16]P. Lopez, Y. S. Ryzantsev, R. G. Rubio, F. Ortega, M. G. Velarde, and J. M. Redondo, "Observation of the thermocapillary motion of a droplet in a laser beam," in *Without Bounds: A Scientific Canvas of Nonlinearity and Complex Dynamics*, edited by R. G. Rubio (Springer, 2013).

[17]J. M. Rendondo, P. Lopez, O. B. Mahjoub, Y. S. Ryazantsev, and M. G. Velarge, "Thermocapilarity and radiative heat flux oscillations," in Topical Problems of Fluid Mechanics, Prague, 2014.

[18]Y. S. Ryazantsev, M. G. Velarde, R. G. Rubio, E. Guzman, F. Ortega, and P. Lopez, "Thermo- and soluto-capillarity: Passive and active drops," Adv. Coll. Interface Sci. **247**, 52 (2017).

[19]B. Zhang, D. Liu, Y. Chen, J. Xu, and Y. Sui, "Numerical investigation on spontaneous droplet/bubble migration under thermal radiation," Int. J. Therm. Sci. **129**, 115 (2018).

[20]J.-H. Gao and Z.-B. Wu, "Steady thermocapillary droplet migration under thermal radiation with a uniform flux," Microgravity Sci. Tech. **33**, 5 (2021).

[21]D. A. Edwards, H. Brenner, and D. T. Wasan, *Interfacial Transport Processes and Rheology* (Butterworth-Heiemann, 1961).

[22]L. E. Scriven, "Dynamics of a fluid interface: Equation of motion for Newtonian surface fluids," Chem. Eng. Sci. **19**, 98 (1960).

[23]J. F. Happer, D. W. Moore, and J. R. A. Pearson, "The effect of the variation of surface tension with temperature on the motion of bubbles and drops," J. Fluid Mech. **27**, 361 (1967).

[24]F. E. Torres and E. Herbolzheimer, "Temperature gradients and drag effects produced by convection of interfacial internal energy around bubbles," Phys. Fluids A **5**, 537 (1993).

[25]Z. Khattari, P. Steffen, and T. M. Fischer, "Migration of a droplet in a liquid: Effect of insoluble surfactants and thermal gradient," J. Phys.: Condens. Matter **14**, 4823 (2002).

[26]R. Balasubramaniam and R. S. Subramanian, "Thermocapillary migration of a drop: An exact solution with Newtonian interfacial rheology and stretching/shrinkage of interfacial area elements for small Marangoni numbers," Ann. N. Y. Acad. Sci. **1027**, 303 (2004).

[27]J. T. Schwalbe, F. R. Phelan, P. M. Vlahovska, and S. D. Hudson, "Interfacial effects on droplet dynamics in Poiseuille flow," Soft Matter **7**, 7797 (2011).

[28]S. Das and S. Chakraborty, "Influence of complex interfacial rheology on the thermocapillary migration of a surfactant-laden droplet in Poiseuille flow," Phys. Fluids **30**, 022103 (2018).

[29]V. Narsimhan, "Letter: The effect of surface viscosity on the translational speed of droplets," Phys. Fluids **30**, 081703 (2018).

[30]S. N. Jadhav and U. Ghosh, "Effect of interfacial kinetics on the settling of a drop in a viscous medium," Phys. Fluids **34**, 042007 (2022).

[31]J.-P. Delville, M. Vincent, R. Schroll, H. Chraibi, B. Issenmann, R. Wunenburger, D. Lasseux, W. W. Zhang, and E. Brasselet, "Laser microfluidics: Fluid actuation by light," J. Opt. A: Pure Appl. Opt. **11**, 034015 (2009).

[32]A. Karbalaei, R. Kumar, and H. J. Cho, "Thermocapillary in microfluidics: A review," Micromachines **7**, 13 (2016).

[33]S. Rybalko, N. Magome, and K. Yoshikawa, "Forward and backword laser-guided motion of an oil droplet," Phys. Rev. E **70**, 046301 (2004).

[34]C. N. Baroud, J.-P. Delville, F. Gallaire, and R. Wunenburger, "Thermocapillary value for droplet production and sorting," Phys. Rev. E **75**, 046302 (2007).

[35]M. Muto, A. Hosi, M. Yamamoto, and M. Motosuke, "Microfluidic droplet manipulation by phorothermal interfacial flow," Trans. Visualization Soc. Jpn. **36**, 8 (2016).

[36]Y. Xiao, S. Zarghami, K. Wagner, P. Wagner, K. Gordon, L. Florea, D. Diamond, and D. Officer, "Moving droplets in 3D using light," Adv. Mater. **30**, 1801821 (2018).

[37]Z.-B. Wu and W. R. Hu, "Effects of Marangoni numbers on thermocapillary droplet migration: Constant for quasi-steady state?," J. Math. Phys. **54**, 023102 (2013).

[38]Z.-B. Wu, "Steady thermocapillary migration of a droplet in a uniform temperature gradient combined with a radiation energy source at large Marangoni numbers," Phys. Rev. E **98**, 013110 (2018).

[39]Z.-B. Wu, "Thermocapillary droplet migration in a vertical temperature gradient controlled by thermal radiations," Phys. Fluids **34**, 022109 (2022).

[40]Z. B. Wu, "Thermocapillary migration of a planar droplet at small and large Marangoni numbers: Effects of interfacial rheology," Z. Angew. Math. Phys. **71**, 8 (2020).

[41]J. Happel and H. Brenner, *Low Reynolds Number Hydrodynamics* (Prentice-Hall, 1965).

[42]Z.-X. Wang and D.-R. Guo, *Special Functions* (World Scientific, 1989).

[43]P. H. Hadland, R. Balasubramaniam, and G. Wozniak, "Thermocapillary migration of bubbles and drops at moderate to large Marangoni number and moderate Reynolds number in reduced gravity," Exp. Fluid **26**, 240 (1999).

[44]J. C. Xie, H. Lin, P. Zhang, F. Liu, and W. R. Hu, "Experimental investigation on thermocapillary drop migration at large Marangoni number in reduced gravity," J. Coll. Interface Sci. **285**, 737 (2005).